

FAST SOLUTION OF SYLVESTER-STRUCTURED SYSTEMS FOR SPATIAL SOURCE SEPARATION OF THE COSMIC MICROWAVE BACKGROUND

DUNG PHAM, KIRK M. SOODHALTER, AND SIMON WILSON

ABSTRACT. Implementation of many statistical methods for large, multivariate data sets requires one to solve a linear system that, depending on the method, is of the dimension of the number of observations or each individual data vector. This is often the limiting factor in scaling the method with data size and complexity. In this paper we illustrate the use of Krylov subspace methods to address this issue in a statistical solution to a source separation problem in cosmology where the data size is prohibitively large for direct solution of the required system. Two distinct approaches, adapted from techniques in the literature, are described: one that uses the method of conjugate gradients directly to the Kronecker-structured problem and another that reformulates the system as a Sylvester matrix equation. We show that both approaches produce an accurate solution within an acceptable computation time and with practical memory requirements for the data size that is currently available.

1. INTRODUCTION

In this paper we describe an approach to solving a sparse, high-dimensional linear system that arises in the context of a particular form of the statistical model known as factor analysis [3], also known in the machine learning literature as independent components analysis [5, Chapter 12]. This model is used in the analysis of multivariate data, most commonly for:

- Dimension reduction – identifying a lower dimensional linear subspace of the data space that still captures a large amount of the data variation, to which further analysis is then applied. This is one approach to handling data whose dimension makes analysis computationally infeasible;

Date: September 27, 2024.

2010 Mathematics Subject Classification. 65F10, 65F50, 65F08.

Key words and phrases. Cosmic Microwave Background, Gaussian field, Krylov subspace, source separation, Conjugate Gradients, Sylvester Equations.

- Interpretation – identifying linear combinations of data components that are able to be interpreted in some way, for the purposes of gaining insights into the data generating process or learning about those linear combinations. One application of this is source separation, the motivating example for this work.

This work is motivated by a problem arising out of data analysis in cosmology. Our approach makes use of Krylov subspaces. Methods built on these subspaces have been used to apply statistical methods to scale to larger data sets, starting with [27] and then in a series of papers to [1]. Like this work, those papers focused on the problems associated with working with high-dimensional Gaussian distributions, where statistical inference and prediction usually involve operations on its variance matrix that is the dimension of the data. This matrix is often designed to be sparse and hence suited to Krylov subspace methods. In the specific context of CMB reconstruction, Krylov subspace iterative methods employing subspace recycling acceleration have been used to great effectiveness [18].

This paper is organised as follows. Section 2 discusses the source separation problem for the Cosmic Microwave Background, the motivating example that led to this work. Section 3 describes our approaches to solving the linear system that arises out of the example, which are then evaluated in Section 4. Section 5 contains some concluding remarks.

2. MOTIVATING EXAMPLE

One of the most important scientific discoveries of the past century was undoubtedly the observation of the cosmic microwave background (CMB); see [20]. The discovery is one of the strongest pieces of evidence for the Big Bang theory, which predicted its existence. The properties of the CMB carry important information about how the universe has evolved from very early epochs, and therefore there is great interest in making a full sky measurement of CMB as accurately as possible. To date, three satellites -- COBE, WMAP and most recently Planck -- have done this with increasing sensitivity and resolution. Planning for a future mission that would make even more detailed observations has started [8].

An important problem is that the signals measured by these satellites do not contain only CMB radiation but also contributions from a number of other microwave sources. Hence the contribution of CMB to the observed microwave brightness at any point in the sky must be separated out. These other sources come in two types. There are point sources, consisting of stars and galaxies; these are relatively easy to identify and remove from the data. There are also diffuse sources, such as microwaves emitted from dust in our galaxy. These are harder to separate from the CMB, which is also a diffuse signal. The source separation problem concerns these diffuse sources only, assuming that the point sources have been removed prior to analysis.

2.1. SOURCE SEPARATION MODEL FOR ALL-SKY MAPS. This source separation problem can be formulated as follows. There are n all-sky maps of microwave brightnesses that have been observed at frequencies ν_1, \dots, ν_n . These maps consist of a discrete grid of values over N pixels that partition the entire sky. In astronomy, the HEALPix partition into pixels of equal area is used [11]. HEALPix partitions the sky into 12 ‘base’ areas, and a separate analysis is done on each; see Appendix A for more details. For Planck data, $n = 9$ and there are 12 base areas each with $N = 4^{10} = 1,048,576$ pixels, for a total of 12,582,912 pixels across the entire sky. The following analysis is repeated 12 times for each base patch and the results are stitched together.

Let $\mathbf{y}_j \in \mathbb{R}^n$ denote the brightness of the maps at pixel j . Assuming that point sources have been dealt with, the brightness at each point in the sky is a combination of the m different diffuse sources. Letting $\mathbf{s}_j \in \mathbb{R}^m$ denote the vector of source brightnesses at pixel j , the source separation model takes the form:

$$(1) \quad \mathbf{y}_j = \mathbf{A}\mathbf{s}_j + \boldsymbol{\epsilon}_j, \quad j = 1, \dots, N,$$

where \mathbf{A} is an $n \times m$ matrix of weights (known as the mixing matrix in source separation) and $\boldsymbol{\epsilon}_j$ is a vector of independent measurement errors, assumed to be independently Gaussian distributed with mean 0 and known variances $\sigma_1^2, \dots, \sigma_n^2$. In the full inference task, \mathbf{A} is defined by a small number of parameters whose values must be learned from the data. Because that aspect of the learning task is not relevant to this work, here

the elements of \mathbf{A} are assumed to have known values. Appendix B gives the details of the construction of \mathbf{A} .

Let $\mathbf{y}_k = (y_{1k}, \dots, y_{Nk})$ denote the k th map (in other words, the k th component of each \mathbf{y}_j) and $\mathbf{Y} = (\mathbf{y}_1, \dots, \mathbf{y}_n) \in \mathbb{R}^{nN}$ denote the vector of all observations, stacked by map. Similarly $\mathbf{s}_l = (s_{1l}, \dots, s_{Nl})$ is the map of the l th source and $\mathbf{S} = (\mathbf{s}_1, \dots, \mathbf{s}_m) \in \mathbb{R}^{mN}$. Following Equation 1, one has

$$\mathbf{Y} = \mathbf{B}\mathbf{S} + \boldsymbol{\varepsilon},$$

where $\mathbf{B} = \mathbf{A} \otimes \mathbf{I}_N$ is an $nN \times mN$ matrix, \mathbf{I}_N is the N dimensional identity matrix, and $\boldsymbol{\varepsilon}$ is the vector of nN Gaussian distributed measurement errors with mean vector 0 and $nN \times nN$ dimensional diagonal precision matrix \mathbf{C} , with the first N entries on the diagonal equal to $1/\sigma_1^2$, the next N equal to $1/\sigma_2^2$, and so on. Hence, given \mathbf{A} , \mathbf{S} and the σ_k^2 , \mathbf{Y} is Gaussian distributed with mean $\mathbf{B}\mathbf{S}$ and precision matrix \mathbf{C} :

$$(2) \quad p(\mathbf{Y} | \mathbf{S}) = (2\pi)^{Nn/2} |\mathbf{C}|^{1/2} \exp \left\{ -\frac{1}{2} (\mathbf{Y} - \mathbf{B}\mathbf{S})^T \mathbf{C} (\mathbf{Y} - \mathbf{B}\mathbf{S}) \right\}.$$

Note that, for Planck data, $nN = 9 \times 4^{10} = 9,437,184$ and typically one uses $m = 4$ diffuse sources so that $mN = 4 \times 4^{10} = 4,194,304$.

The final element of the problem is a model for the diffuse sources. In a Bayesian learning approach, this model is a probability distribution $p(\mathbf{S})$, known as the prior distribution, that serves to regularise the separation task. In our approach, this distribution models the spatial smoothness of each diffuse source through the use of an intrinsic Gaussian Markov random field model [21]. This model ensures that the intensity of a source at neighbouring pixels in the sky cannot be too different; more concretely, if pixel j and j' are neighbours then $y_{jk} - y_{j'k}$ is zero-mean Gaussian distributed with a variance φ_k whose value must be specified. The different source maps are assumed to be independent. This leads to a zero-mean multivariate Gaussian form for $p(\mathbf{S})$ with a block diagonal form for the covariance matrix \mathbf{Q}^{-1} , one block being associated with each source:

$$(3) \quad p(\mathbf{S}) = (2\pi)^{Nm/2} |\mathbf{Q}|^{1/2} \exp \left\{ -\frac{1}{2} (\mathbf{Y} - \mathbf{B}\mathbf{S})^T \mathbf{Q} (\mathbf{Y} - \mathbf{B}\mathbf{S}) \right\},$$

where $\mathbf{Q} = \text{bldiag}(\mathbf{Q}_1(\varphi_1), \dots, \mathbf{Q}_m(\varphi_m))$ is an $mN \times mN$ matrix and the $\mathbf{Q}_l(\varphi_l)$ are sparse, positive semi-definite $N \times N$ matrices, each depending on a single parameter φ_l . Appendix C has details on the form and derivation of the \mathbf{Q}_l .

2.2. SOURCE SEPARATION SOLUTION. The primary task is to use the data \mathbf{Y} to learn about all sources \mathbf{S} . A Bayesian learning approach is adopted, where the goal is to derive the so-called posterior probability distribution $p(\mathbf{S}|\mathbf{Y})$. Following Bayes' Law:

$$p(\mathbf{S}|\mathbf{Y}) \propto p(\mathbf{Y}|\mathbf{S})p(\mathbf{S}),$$

where Equations 2 and 3 specify $p(\mathbf{Y}|\mathbf{S})$ and $p(\mathbf{S})$.

Some simple properties of the Gaussian distribution show that $p(\mathbf{S}|\mathbf{Y})$ is another Gaussian with precision matrix

$$(4) \quad \hat{\mathbf{Q}} = \mathbf{B}^T \mathbf{C} \mathbf{B} + \mathbf{Q}$$

and mean vector $\hat{\boldsymbol{\mu}}$ that satisfies

$$(5) \quad \hat{\mathbf{Q}} \hat{\boldsymbol{\mu}} = \mathbf{B}^T \mathbf{C} \mathbf{Y}.$$

So key to implementing the source separation is the solution to Equation 5, under the structures for \mathbf{Q} , \mathbf{B} and \mathbf{C} that have been described, as this gives a point estimate of the sources. In addition, computing elements of $\hat{\mathbf{Q}}$ (of most importance being the main diagonal that contains the variance of the sources at each pixel) gives information about uncertainty of and correlation between source values across the sky. We elaborate on implementing the action of $\hat{\mathbf{Q}}$ in the subsequent section.

3. SOLVING THE LINEAR SYSTEM

Although \mathbf{Q} is only semi-positive definite, $\hat{\mathbf{Q}}$ will be positive definite. As is often the case, the sparsity of $\hat{\mathbf{Q}}$ does not guarantee that its Cholesky decomposition will be sparse. One could consider sparse direct methods (see, e.g., [10]) in this setting, but this problem has so much additional structure that we explore matrix-free approaches which take advantage of Kronecker structure. Thus, we do not consider sparse-direct methods in this paper, though we do use SuperLU [14, 12, 13] as an inner solver for a method suggested in [4] against which we test our proposed

solvers, cf. Section 4.4. We also note that our descriptions of quantities arising in Kronecker form and the use reshaping to map between Kronecker form and unvectorised form is only a matter of presentation. We do not advocate reshaping to go between Kronecker and unvectorised forms.

The problem being solved is of the form

$$(6) \quad (\mathbf{Q} + \mathbf{B}^T \mathbf{C} \mathbf{B}) \boldsymbol{\mu} = \mathbf{B}^T \mathbf{C} \mathbf{Y} \quad \text{with} \quad (\mathbf{Q} + \mathbf{B}^T \mathbf{C} \mathbf{B}) \in \mathbb{R}^{mN \times mN}$$

where $m \in \{4, 5\}$ and $N = \mathcal{O}(10^7)$. As described in Appendix C, \mathbf{Q} is a m -block diagonal matrix with block i being of the form $\mathbf{Q}_i(\varphi_i) = \varphi_i \mathbf{D}^T \mathbf{D} = \varphi_i \mathbf{D}^2$, for $\varphi_i > 0$. The matrix $\mathbf{D} \in \mathbb{R}^{N \times N}$ is symmetric and its elements encode a nearest neighbor coupling of nodes from the discretization of the sky, whereby

$$\mathbf{D} = (D_{ij}) \quad \text{with} \quad D_{j_1, j_2} = \begin{cases} 1 & \text{nodes } j_1 \neq j_2 \text{ are neighbors} \\ 0 & \text{nodes } j_1 \neq j_2 \text{ are not neighbors} \\ -\sum_{\ell \neq j}^N D_{j\ell} & j := j_1 = j_2 \end{cases}$$

The matrix $\mathbf{B} \in \mathbb{R}^{nN \times mN}$ with $n = 9$ can be written as the Kronecker product $\mathbf{B} = \mathbf{A} \otimes \mathbf{I}_N$ where $\mathbf{A} \in \mathbb{R}^{n \times m}$. We also have that $\mathbf{C} \in \mathbb{R}^{nN \times nN}$ is a diagonal matrix with all positive entries. The matrix \mathbf{C} also has Kronecker structure; namely, there are N positive integer values n_1, \dots, n_N and n positive values τ_1, \dots, τ_n

$$\mathbf{C} = \text{diag}\{\tau_1, \tau_2, \dots, \tau_n\} \otimes \text{diag}\{n_1, n_2, \dots, n_N\} =: \mathbf{T} \otimes \mathbf{N}.$$

We propose treating this problem using iterative methods built on efficient implementations of matrix-vector products (matvecs) for the matrices from this problem (cf. section 3.2) or as the low-rank approximation to the solution of a Sylvester matrix equation (cf. section 3.3). Furthermore, most of the system matrix should never be explicitly constructed. Rather, it should only be represented as a stored procedure implementing matrix-vector product. The only matrix explicitly represented should be \mathbf{A} .

3.1. EFFICIENT MATRIX-VECTOR PRODUCTS. We describe first how to perform the matrix-vector product for each part of the full system matrix and then we finish by combining them, yielding a routine for $\mathbf{x} \mapsto (\mathbf{Q} + \mathbf{B}^T \mathbf{C} \mathbf{B}) \mathbf{x}$. This will be necessary for

using an appropriate iterative method whose core operation is this matvec routine. Observe that since \mathbf{D} is a sparse matrix encoding the nearest-neighbor coupling for each node, the routine $\mathbf{v} \mapsto \mathbf{D}\mathbf{v}$ involves updating entry j of \mathbf{v} (associated to node j of grid) using its four nearest neighbors and the value at the node itself. Thus a sequential matrix-free routine can be easily formulated. For Algorithm 1,

ALGORITHM 1: Matvec procedure $\mathbf{v} \mapsto \mathbf{D}\mathbf{v}$	
1	Given: vector $\mathbf{v} \in \mathbb{R}^N$, perhaps represented as nodal values on the grid
2	FOR $j = 1, 2, \dots, N$ DO
3	$\mathbf{v}(j) \leftarrow \mathbf{v}(j_{right}) + \mathbf{v}(j_{left}) + \mathbf{v}(j_{above}) + \mathbf{v}(j_{below}) - \left(\sum_{\ell \neq j}^N D_{j\ell} \right) \mathbf{v}(j)$
4	END

we note that since the matrix \mathbf{D} does not change, we can pre-compute and store the rowsums $\sum_{\ell \neq j}^N D_{j\ell}$. Also, it should be noted that Algorithm 1 is parallelizable, as the grid can be divided up and sent to different processes, and communication between processors only needs to occur for neighboring nodes that are on different processors. The computational cost of a serial version of Algorithm 1 is $\mathcal{O}(N)$, since we do 4 floating point operations per entry of \mathbf{v} .

As already discussed, \mathbf{Q} is a block diagonal matrix with blocks $\varphi_i \mathbf{D}^2$. Thus, it can be represented as a Kronecker product, namely

$$\mathbf{Q} = \begin{bmatrix} \varphi_1 & & & \\ & \varphi_2 & & \\ & & \ddots & \\ & & & \varphi_n \end{bmatrix} \otimes \mathbf{D}^2 =: \mathbf{P} \otimes \mathbf{D}^2.$$

For $\mathbf{u} = \mathbf{w} \otimes \mathbf{v} \in \mathbb{R}^{nN}$ with $\mathbf{w} \in \mathbb{R}^n$, we perform this matrix-vector product by instead considering a reshaping of \mathbf{u} . Using the MATLAB-style reshape notation, let $\mathbf{U} = \text{reshape}(\mathbf{u}, N, n) \in \mathbb{R}^{N \times n}$; i.e.,

$$\text{if } \mathbf{u} = \begin{bmatrix} \mathbf{u}_1 \\ \mathbf{u}_2 \\ \vdots \\ \mathbf{u}_n \end{bmatrix} \quad \text{then} \quad \mathbf{U} = \text{reshape}(\mathbf{u}, N, n) = \begin{bmatrix} \mathbf{u}_1 & \mathbf{u}_2 & \cdots & \mathbf{u}_n \end{bmatrix}.$$

Then the matvec in Algorithm 1 can also be represented by reshaping \mathbf{u} and computing $\mathbf{D}^2\mathbf{U}\mathbf{P}$. Again, we take advantage of the Kronecker structures of \mathbf{B} and \mathbf{C} . We can write

$$(7) \quad \mathbf{B}^T \mathbf{C} \mathbf{B} \mathbf{x} = (\mathbf{A}^T \otimes \mathbf{I}_N) (\mathbf{T} \otimes \mathbf{N}) (\mathbf{A} \otimes \mathbf{I}_N) \mathbf{x}.$$

If we set $\mathbf{M} = \text{reshape}(\mathbf{x}, N, n)$, then the matrix-vector product can be efficiently executed via the block vector mapping

$$(8) \quad \mathbf{M} \mapsto (\mathbf{N} (\mathbf{M} \mathbf{A}^T) \mathbf{T}) \mathbf{A},$$

which enables the running of a matrix-free Krylov iteration on a Kronecker-structured system implicitly, without forming any Kronecker products.

3.2. SOLUTION OF EQ. (6) USING MATRIX-FREE ITERATIVE METHODS. The first strategy we propose entails considering the linear system eq. (6) as it is presented with the coefficient matrix being built from and applied implicitly using the Kronecker product formulation. We propose to use a so-called “matrix-free” method which only requires a stored procedure to perform $\mathbf{x} \mapsto (\mathbf{Q} + \mathbf{B}^T \mathbf{C} \mathbf{B}) \mathbf{x}$, implemented in block form via (8), meaning we need no explicit representation of the coefficient matrix.

We briefly review standard Krylov subspace methods and introduce some terminology. For a more detailed description, see, e.g., [24, 26, 29] and the references therein. Consider solving

$$(9) \quad \mathbf{G}(\mathbf{x}_0 + \mathbf{t}) = \mathbf{b}$$

where $\mathbf{G} \in \mathbb{R}^{n \times n}$, $\mathbf{x}_0 \in \mathbb{R}^n$ is an initial approximation, and \mathbf{t} is the unknown correction. Let $\mathbf{r}_0 = \mathbf{b} - \mathbf{G}\mathbf{x}_0$ be the initial residual. In iteration j , a Krylov method selects a correction \mathbf{t}_j from the j th Krylov subspace generated by \mathbf{G} and \mathbf{r}_0 ,

$$(10) \quad \mathbf{t}_j \in \mathcal{K}_j(\mathbf{G}, \mathbf{r}_0) = \text{span} \{ \mathbf{r}_0, \mathbf{G}\mathbf{r}_0, \mathbf{G}^2\mathbf{r}_0, \dots, \mathbf{G}^{j-1}\mathbf{r}_0 \} = \{ p(\mathbf{G})\mathbf{r}_0 \mid \deg p < j \},$$

i.e., from the space of polynomials of degree less than j in \mathbf{G} acting on \mathbf{r}_0 . The constraint space defines the Krylov subspace method up to implementation choices and must also be compatible with the correction space such that the method being

implicitly defined can be efficiently implemented and exhibits good convergence characteristics.

For coefficient matrices \mathbf{G} that are symmetric positive definite (such as that in eq. (6)), the celebrated, efficient, and stable method of Conjugate Gradients is the Krylov subspace method of choice. Implicitly, at iteration j , the method has generated the subspace $\mathcal{K}_j(\mathbf{G}, \mathbf{r}_0)$ and computes $\mathbf{t}_j \in \mathcal{K}_j(\mathbf{G}, \mathbf{r}_0)$ such that the approximation $\mathbf{x}_j = \mathbf{x}_0 + \mathbf{t}_j$ minimizes

$$\|\mathbf{x} - \mathbf{x}_j\|_G^2 = \|\mathbf{b} - \mathbf{G}\mathbf{x}_j\|_{G^{-1}}^2 = (\mathbf{b} - \mathbf{G}\mathbf{x}_j)^T \mathbf{G}^{-1} (\mathbf{b} - \mathbf{G}\mathbf{x}_j).$$

The actual derivation of the method can be found in, e.g., [24]. We note that we have omitted a Lanczos-based derivation of CG, as its derivation is well documented in the literature. We derive an alternative approach based on block Lanczos in Section 3.3. We present CG for the case $\mathbf{G} = (\mathbf{Q} + \mathbf{BCB}^T)$ and right-hand side $\mathbf{b} = \mathbf{B}^T \mathbf{C} \mathbf{Y}$ as Algorithm 2.

ALGORITHM 2: Method of Conjugate Gradients - for $\mathbf{G} = (\mathbf{Q} + \mathbf{BCB}^T)$ and $\mathbf{b} = \mathbf{B}^T \mathbf{C} \mathbf{Y}$	
1	Given: \mathbf{y} , \mathbf{B} , \mathbf{C} , and \mathbf{Q} defined as above and \mathbf{x}_0 ; $\varepsilon > 0$ a convergence tolerance
2	$\mathbf{x} = \mathbf{x}_0$; $\mathbf{r} = \mathbf{BCy} - (\mathbf{Q} + \mathbf{BCB}^T) \mathbf{x}$; $\mathbf{p} = \mathbf{r}_0$
3	WHILE $\ \mathbf{r}\ > \varepsilon \ \mathbf{r}_0\ $ DO
4	$\mathbf{r}_{old} \leftarrow \mathbf{r}$
5	$\mathbf{q} \leftarrow (\mathbf{Q} + \mathbf{BCB}^T) \mathbf{p}$
6	$\alpha = \frac{\mathbf{r}^T \mathbf{r}}{\mathbf{p}^T \mathbf{q}}$
7	$\mathbf{x} \leftarrow \mathbf{x} + \alpha \mathbf{p}$
8	$\mathbf{r} \leftarrow \mathbf{r} - \alpha \mathbf{q}$
9	$\beta \leftarrow \frac{\mathbf{r}^T \mathbf{r}}{\mathbf{r}_{old}^T \mathbf{r}_{old}}$
10	$\mathbf{p} \leftarrow \mathbf{r} + \beta \mathbf{p}$
11	END

ADVANTAGES. The CG methods has a number of advantages in this setting. The coefficient matrix of eq. (6) does not need to be constructed (and there is no expensive decomposition). The convergence speed is determined by the eigenvalues of the coefficient matrix and the specific right-hand side. If convergence speed is too slow, preconditioning techniques can be used to accelerate convergence. Furthermore, in this setting CG is quite amenable to parallelization by distributing sky domain grid onto different processors and parallelizing matvec procedures.

DISADVANTAGES. The CG method also has some relevant disadvantages in this setting. We still must deal with vectors of size nN . We also cannot take advantage of any structure or compressibility which may be present in \mathbf{Y} . Most importantly, it has been shown that applying an iterative method directly to the tensor-structured problem can lead to performance hampered by the large condition number of the full-size problem [17].

Understanding both the advantages and disadvantages, we have been able to demonstrate for this problem using real data that the CG method can be used effectively to solve the problem. One observation we make is that the coefficient matrix arises from the Bayesian regularisation of the source separation problem. Such matrices are often more well-conditioned due to the regularisation.

3.3. SOLUTION OF EQ. (6) USING A SYLVESTER INTERPRETATION. Going one step further, we can simply reshape eq. (6) and interpret directly as a Sylvester matrix equation, which will allow us to take advantage of additional structure in \mathbf{y} that may be available.

We can reshape the solution ($\mathbf{M} = \text{reshape}(\boldsymbol{\mu}, N, n)$) and ($\mathbf{Y} = \text{reshape}(\mathbf{y}, N, m)$). With these reshapings, we can rewrite eq. (6) as the generalize Sylvester equation

$$\mathbf{D}^2\mathbf{M}\mathbf{P} + \mathbf{N}\mathbf{M}\mathbf{A}^T\mathbf{T}\mathbf{A} = \mathbf{N}\mathbf{Y}\mathbf{T}\mathbf{A}.$$

As \mathbf{N} and \mathbf{P} are diagonal and invertible, we can easily multiply on the left by \mathbf{N}^{-1} and on the right by \mathbf{P}^{-1} , yielding the Sylvester equation

$$(11) \quad \mathbf{N}^{-1}\mathbf{D}^2\mathbf{M} + \mathbf{M}\mathbf{A}^T\mathbf{T}\mathbf{A}\mathbf{P}^{-1} = \mathbf{Y}\mathbf{T}\mathbf{A}\mathbf{P}^{-1}.$$

A survey by Simoncini covering a variety of solution techniques was recently published [25]. Since $\mathbf{A}^T\mathbf{T}\mathbf{A}\mathbf{P}^{-1} \in \mathbb{R}^{n \times n}$, this falls into a category of Sylvester equations with one large, sparse coefficient matrix ($\mathbf{N}^{-1}\mathbf{D}^2$) and one small, dense one ($\mathbf{A}^T\mathbf{T}\mathbf{A}\mathbf{P}^{-1}$). Following [4], we denote this as sparse-dense category. We describe a technique from the literature wherein this structure has been previously exploited.

3.3.1. *An existing technique for the treating sparse-dense Sylvester equations.* Since (11) falls into this category, it is of the form

$$(12) \quad \mathbf{H}\mathbf{M} + \mathbf{M}\mathbf{L} = \mathbf{F},$$

with \mathbf{H} large and sparse and \mathbf{L} small and dense. In [4], the authors propose Algorithm 3 to solve (12). In the numerical experiments (cf. Section 4.4), we demonstrate that this algorithm is not appropriate for the full-scale application problem we are treating in this manuscript. For small problems, it does produce solutions with smaller residual norms than what we propose in the subsequent section, but it exhibits quadratic growth in solve time as we increase the problem size, mainly due to the cost of inner linear solves required by method; see Section 4.4 for further details.

We propose a different approach, which we demonstrate (for test problems involving real Planck data) is more robust with respect to the increase in run time as the size of the problem (i.e., size of the data) increases, and we demonstrate that it delivers solutions with sufficient accuracy in a timely manner. It uses the fact that equations with Sylvester structure can be treated using block Krylov subspaces, exploiting a block generalization of the shift-invariance exhibited by Krylov subspaces; see, e.g., [9] concerning shift invariance and [25] and references therein for its block generalization to the Sylvester equation setting.

ALGORITHM 3: Solution of the Sparse-Dense Sylvester Equation (from [4])	
1	INPUT: $\mathbf{H} \in \mathbb{R}^{N \times N}, \mathbf{L} \in \mathbb{R}^{n \times n}$ and $\mathbf{F} \in \mathbb{R}^{N \times n}$ defining (12)
2	OUTPUT: $\mathbf{M} \in \mathbb{R}^{N \times n}$ SOLVING (12)
3	Compute Schur decomposition $\mathbf{L} = \mathbf{W}\mathbf{R}\mathbf{W}^T, \mathbf{W}^T\mathbf{W} = \mathbf{I}_n$
4	$\hat{\mathbf{F}} := \mathbf{F}\mathbf{W}$
5	FOR $i = 1, 2, \dots, n$ DO
6	$\hat{\mathbf{F}} := \mathbf{F}_i - \sum_{k=1}^{i-1} \hat{\mathbf{X}}_k R_{ki}$
7	Solve $(\mathbf{H} + R_{ii}\mathbf{I})\hat{\mathbf{X}}_i = \hat{\mathbf{F}}$
8	END
9	$\mathbf{M} := \hat{\mathbf{X}}\mathbf{W}$
10	RETURN \mathbf{M}

3.3.2. *Application of block Krylov approach for large-scale problems.* Large-scale Sylvester-structured problems of sparse-dense type are amenable to solution by generating a block Krylov subspace associated to the large coefficient matrix, i.e.,

$\mathbf{N}^{-1}\mathbf{D}^2$. This space at iteration j has the form

$$\begin{aligned}\mathbb{K}_j(\mathbf{N}^{-1}\mathbf{D}^2, \mathbf{YTA}\mathbf{P}^{-1}) &:= \mathcal{K}_j(\mathbf{N}^{-1}\mathbf{D}^2, \mathbf{YTA}\mathbf{e}_1) \\ &\quad + \mathcal{K}_j(\mathbf{N}^{-1}\mathbf{D}^2, \mathbf{YTA}\mathbf{e}_2) + \dots \\ &\quad + \mathcal{K}_j(\mathbf{N}^{-1}\mathbf{D}^2, \mathbf{YTA}\mathbf{e}_m),\end{aligned}$$

where \mathbf{e}_i is the i th Cartesian basis vector. The Sylvester equation is projected onto this space, and a smaller Sylvester problem is solved at each iteration. The matrix $\mathbf{N}^{-1}\mathbf{D}^2$ is no longer symmetric positive definite in the standard inner product; however, it is if we consider a different inner product.

Any symmetric positive-definite matrix can be used to define a new inner product. The matrix \mathbf{N} is a diagonal matrix with only positive entries on its diagonal; therefore, it is a positive-definite matrix and can be used to induce the inner product $(\mathbf{x}, \mathbf{y})_{\mathbf{N}} = \mathbf{y}^T \mathbf{N} \mathbf{x}$. A matrix \mathbf{G} is symmetric with respect to $(\cdot, \cdot)_{\mathbf{N}}$ if for all $\mathbf{x}, \mathbf{y} \in \mathbb{R}^n$ $(\mathbf{G}\mathbf{x}, \mathbf{y})_{\mathbf{N}} = (\mathbf{x}, \mathbf{G}\mathbf{y})_{\mathbf{N}}$; i.e., $\mathbf{y}^T \mathbf{N} \mathbf{G} \mathbf{x} = \mathbf{y}^T \mathbf{G}^T \mathbf{N} \mathbf{x}$.

What is important here is that we exploit the property proven in the following Lemma.

LEMMA 3.1. *The coefficient matrix $\mathbf{N}^{-1}\mathbf{D}^2$ is symmetric with respect to $(\cdot, \cdot)_{\mathbf{N}}$.*

Proof. This is straightforward to show by direct computation. For all $\mathbf{x}, \mathbf{y} \in \mathbb{R}^n$, we have

$$(\mathbf{N}^{-1}\mathbf{D}^2\mathbf{x}, \mathbf{y})_{\mathbf{N}} = \mathbf{y}^T \mathbf{N} \mathbf{N}^{-1} \mathbf{D}^2 \mathbf{x} = \mathbf{y}^T \mathbf{D}^2 \mathbf{x} = \mathbf{y}^T \mathbf{D}^2 \mathbf{N}^{-1} \mathbf{N} \mathbf{x} = (\mathbf{x}, \mathbf{N}^{-1} \mathbf{D}^2 \mathbf{y})_{\mathbf{N}}.$$

Thus the symmetry with respect to $(\cdot, \cdot)_{\mathbf{N}}$ is proven. \square

Iterative methods designed for symmetric matrices can be converted to methods for matrices symmetric with respect to any inner product simply by using that inner product in the algorithm. We can implement a Conjugate Gradient-like iteration which uses a fixed amount of memory, is amenable to parallelization, and can be implemented to have good data movement characteristics 1/ Thus it behooves us to elaborate on block Lanczos-based methods for symmetric matrices.

1/ For problems of this size, we must concern ourselves with how much data an algorithm moves, as this becomes a dominating cost.

3.3.3. *The block Lanczos process with respect to $(\cdot, \cdot)_{\mathbf{N}}$.* We mentioned in Section 3.2 that CG is a Krylov subspace method. However, we avoided describing any of the details about how this subspace is used to derive CG for brevity. We elaborate here on some aspects of Krylov subspaces for symmetric coefficient matrices to derive an iterative method for Sylvester equations whose larger coefficient matrix (here $\mathbf{N}^{-1}\mathbf{D}^2$) is symmetric with respect to $(\cdot, \cdot)_{\mathbf{N}}$.

Let us denote $\hat{\mathbf{Y}} = \mathbf{Y}\mathbf{T}\mathbf{A}\mathbf{P}^{-1}$ and $\hat{\mathbf{L}} = \mathbf{A}^T\mathbf{T}\mathbf{A}\mathbf{P}^{-1}$. The symmetric Lanczos process is an iterative procedure to generate an \mathbf{N} -orthonormal basis for $\mathbb{K}_j(\mathbf{N}^{-1}\mathbf{D}^2, \hat{\mathbf{Y}})$ block-by-block. What has been shown is that if the matrix is symmetric with respect to the inner product used for orthogonalization, at step i , the $(i+1)$ st block of vectors generated at that step are already orthogonal with respect to all but blocks i and $i-1$, meaning the orthogonalization procedure requires we only store the two most recently generated blocks. At step i , we have generated the orthonormal basis $\{\mathbf{V}_1, \mathbf{V}_2, \dots, \mathbf{V}_i\}$ with $\mathbf{V}_\ell \in \mathbb{R}^{n \times m}$, $\mathbf{V}_\ell^T \mathbf{N} \mathbf{V}_k = \mathbf{0}$ for $\ell \neq k$, and $\mathbf{V}_\ell^T \mathbf{N} \mathbf{V}_\ell = \mathbf{I}_m$, the $m \times m$ identity matrix. To obtain the next basis vector, we compute $\mathbf{W}_{i+1} = (\mathbf{N}^{-1}\mathbf{D}^2) \mathbf{V}_i$. Normally, we would then need to orthogonalize these vectors against all previous, but since $\mathbf{N}^{-1}\mathbf{D}^2$ is symmetric with respect to $(\cdot, \cdot)_{\mathbf{N}}$, it has been proven that $\mathbf{V}_\ell^T \mathbf{N} \mathbf{W}_{i+1} = \mathbf{0}$ for $\ell < i-1$. The orthogonalization coefficients are stored in the matrix $\underline{\mathbf{T}}_j \in \mathbb{R}^{(j+1)m, jm}$ whose first jm rows are the symmetric, block tridiagonal matrix $\mathbf{T}_j \in \mathbb{R}^{jm \times jm}$. These have the structure

$$\underline{\mathbf{T}}_j = \begin{bmatrix} \mathbf{H}_1 & \mathbf{B}_2 & & & \\ \mathbf{B}_2 & \mathbf{H}_2 & \mathbf{B}_3 & & \\ & \mathbf{B}_3 & \ddots & \ddots & \\ & & \ddots & \mathbf{H}_{j-1} & \mathbf{B}_j \\ & & & \mathbf{B}_j & \mathbf{H}_j \\ & & & & \mathbf{B}_{j+1} \end{bmatrix} \quad \text{and} \quad \mathbf{T}_j = \begin{bmatrix} \mathbf{H}_1 & \mathbf{B}_2 & & & \\ \mathbf{B}_2 & \mathbf{H}_2 & \mathbf{B}_3 & & \\ & \mathbf{B}_3 & \ddots & \ddots & \\ & & \ddots & \mathbf{H}_{j-1} & \mathbf{B}_j \\ & & & \mathbf{B}_j & \mathbf{H}_j \end{bmatrix},$$

where each block represents an $m \times m$ matrix. The diagonal and super-diagonal blocks represent coefficients that are related to orthogonalization and the subdiagonal blocks represent blocks related to normalization. The symmetry tells us that the normalization block \mathbf{B}_{i+1} , generated when normalizing \mathbf{V}_{i+1} , can be reused as an orthogonalization coefficient at step $i+1$, where it can be shown that in exact

arithmetic

$$(13) \quad \mathbf{V}_{i+1}\mathbf{B}_{i+1} = \mathbf{N}^{-1}\mathbf{D}^2\mathbf{V}_i - \mathbf{V}_i\mathbf{H}_i - \mathbf{V}_{i-1}\mathbf{B}_i.$$

We denote $\mathbf{V}_j = [\mathbf{V}_1, \mathbf{V}_2, \dots, \mathbf{V}_j] \in \mathbb{R}^{N \times jm}$ to be the matrix whose columns are the block Lanczos vectors. In terms of the matrix \mathbf{T}_j , we can use eq. (13) to derive the Lanczos relation, relating $\mathbf{N}^{-1}\mathbf{D}^2$, \mathbf{V}_j , and \mathbf{T}_j ,

$$(14) \quad \mathbf{N}^{-1}\mathbf{D}^2\mathbf{V}_j = \mathbf{V}_{j+1}\mathbf{T}_j.$$

The construction of \mathbf{T}_j is shown as a part of Algorithm 4; see, e.g., [24, 15] for further details. The symmetric Lanczos relation (14) follows directly from the

ALGORITHM 4: Symmetric Lanczos process for iteratively generating a basis for $\mathbb{K}_{j+1}(\mathbf{N}^{-1}\mathbf{D}^2, \hat{\mathbf{Y}})$

```

1 Given: starting block of vectors  $\hat{\mathbf{Y}} \in \mathbb{R}^{N \times m}$ 
2 Out:  $(\cdot, \cdot)_{\mathbf{N}}$ -orthonormal basis  $\{\mathbf{V}_1, \mathbf{V}_2, \dots, \mathbf{V}_{j+1}\}$ 
3 Orthogonalize starting block in  $(\cdot, \cdot)_{\mathbf{N}}$  producing QR-factorization:  $\hat{\mathbf{Y}} =$ 
    $\underbrace{\mathbf{V}_1}_{\in \mathbb{R}^{N \times m}} \underbrace{\mathbf{B}_0}_{\in \mathbb{R}^{m \times m}}$  with  $\mathbf{V}_1^T \mathbf{N} \mathbf{V}_1 = \mathbf{I}_m$ 
4 FOR  $i = 1, 2, \dots, j$  DO
5    $\mathbf{W} \leftarrow \mathbf{N}^{-1}\mathbf{D}^2\mathbf{V}_i$ 
6   IF  $i > 1$  THEN
7      $\mathbf{W} \leftarrow \mathbf{W} - \mathbf{V}_{i-1}\mathbf{B}_i$ 
8   END
9    $\mathbf{H}_i = \mathbf{V}_i^T \mathbf{N} \mathbf{W}$ 
10   $\mathbf{W} \leftarrow \mathbf{W} - \mathbf{V}_i\mathbf{H}_i$ 
11  Orthogonalize  $\mathbf{W}$  in  $(\cdot, \cdot)_{\mathbf{N}}$  producing QR-factorization:  $\mathbf{W} = \mathbf{V}_{i+1}\mathbf{B}_{i+1}$ 
12 END
```

setup of this process. Furthermore, since the columns of \mathbf{V}_j form an \mathbf{N} orthonormal basis for $\mathbb{K}_j(\mathbf{N}^{-1}\mathbf{D}^2, \hat{\mathbf{Y}})$, we have that $\mathbf{V}_j^T \mathbf{N} \mathbf{V}_{j+1} = \begin{bmatrix} \mathbf{I}_{jm} & \mathbf{0} \end{bmatrix}$, and one can then show that,

$$\begin{aligned}
(15) \quad & \mathbf{N}^{-1}\mathbf{D}^2\mathbf{V}_j = \mathbf{V}_{j+1}\mathbf{T}_j \\
& \mathbf{V}_j^T \mathbf{N} \mathbf{N}^{-1}\mathbf{D}^2\mathbf{V}_j = \mathbf{V}_j^T \mathbf{N} \mathbf{V}_{j+1}\mathbf{T}_j \\
& \mathbf{V}_j^T \mathbf{D}^2\mathbf{V}_j = \begin{bmatrix} \mathbf{I}_{jm} & \mathbf{0} \end{bmatrix} \mathbf{T}_j \\
& \mathbf{V}_j^T \mathbf{D}^2\mathbf{V}_j = \mathbf{T}_j,
\end{aligned}$$

which means that \mathbf{T}_j is symmetric.

Building the basis in blocks with the computational kernel being a matrix-times-matrix product and also block orthogonalization produces an algorithm with computationally attractive properties in terms of computational intensity (i.e., the amount of calculations done per unit of data moved into and out of cache) [2, 19], and this is a topic of current study in the context of GPU implementation [6]. Unlike the classical CG approach, though, it is non-trivial to develop a short-recurrence approach to treat symmetric Sylvester equations. However, an effective, efficient approach has been described in the literature.

3.3.4. *Projection methods for Sylvester equations.* Simoncini and Palitta developed a solver for large-scale Sylvester problems where both matrices are symmetric [16, Section 5.2]. We adapt this work to develop a practical method for treating eq. (11). Similar to methods for solving linear systems, we can discretize the Sylvester equations by taking approximations from a subspace and solving a constrained set of equations to determine the specific approximation. In this case, the unknown from eq. (11) is $\mathbf{M} \in \mathbb{R}^{N \times m}$. At step j , we make an approximation of the form

$$(16) \quad \mathbf{M} \approx \mathbf{M}_j = \mathbf{V}_j \mathbf{Z}_j = \sum_{i=1}^j \mathbf{V}_i \mathbf{G}_i \quad \text{where} \quad \mathbf{G}_i \in \mathbb{R}^{m \times m} \quad \text{and} \quad \mathbf{Z}_j = \begin{bmatrix} \mathbf{G}_1 \\ \mathbf{G}_2 \\ \vdots \\ \mathbf{G}_j \end{bmatrix} \in \mathbb{R}^{jm \times m}.$$

Substituting into eq. (11) yields

$$\mathbf{N}^{-1} \mathbf{D}^2 \mathbf{V}_j \mathbf{Z}_j + \mathbf{V}_j \mathbf{Z}_j \hat{\mathbf{L}} \approx \hat{\mathbf{Y}}.$$

We determine \mathbf{Z}_j to be the solution satisfying the equation

$$(17) \quad \mathbf{V}_j^T \mathbf{N} \left(\mathbf{N}^{-1} \mathbf{D}^2 \mathbf{V}_j \mathbf{Z}_j + \mathbf{V}_j \mathbf{Z}_j \hat{\mathbf{L}} \right) = \mathbf{V}_j^T \mathbf{N} \hat{\mathbf{Y}}.$$

Let $\mathbf{E}_1 \in \mathbb{R}^{jm \times m}$ be the matrix with the identity matrix in the first $m \times m$ block and zeros elsewhere. Observing that $\hat{\mathbf{Y}} = \mathbf{V}_1 \mathbf{B}_0 = \mathbf{V}_j \mathbf{E}_1 \mathbf{B}_0$ and using eq. (15), we can simplify eq. (17) as

$$(18) \quad \mathbf{T}_j \mathbf{Z}_j + \mathbf{Z}_j \hat{\mathbf{L}} = \mathbf{E}_1 \mathbf{B}_0.$$

The task has now become to solve a small, fairly dense set of Sylvester equations. We can use standard methods to treat this problem.

We approach eq. (18) by decomposing the matrices \mathbf{T}_j and $\hat{\mathbf{L}}$. The matrix \mathbf{T}_j is symmetric, block-tridiagonal. Thus, we can efficiently compute the eigendecomposition $\mathbf{T}_j = \mathbf{Q}_j \Phi_j \mathbf{Q}_j^T$ where $\mathbf{Q}_j^T \mathbf{Q}_j = \mathbf{I}_j$ and $\Phi_j = \text{diag}\{\phi_1, \phi_2, \dots, \phi_j\}$ is the diagonal matrix of eigenvalues of \mathbf{T}_j . The matrix $\hat{\mathbf{L}}$ is not symmetric with respect to the standard Euclidean inner product. However, we prove it is symmetric with respect to another inner product.

LEMMA 3.2. *The matrix $\hat{\mathbf{L}} = \mathbf{A}^T \mathbf{T} \mathbf{A} \mathbf{P}^{-1}$ is symmetric with respect to the inner product induced by \mathbf{P}^{-1} .*

Proof. The matrix \mathbf{P} is a diagonal matrix with positive entries on the diagonal. Thus it and its inverse are symmetric positive-definite, and \mathbf{P}^{-1} induces the inner product $(\cdot, \cdot)_{\mathbf{P}^{-1}}$, with $(\mathbf{x}, \mathbf{y})_{\mathbf{P}^{-1}} = \mathbf{y}^T \mathbf{P}^{-1} \mathbf{x}$. We can show by direct calculation that $\hat{\mathbf{L}}$ is symmetric with respect to $(\cdot, \cdot)_{\mathbf{P}^{-1}}$,

$$(\mathbf{A}^T \mathbf{T} \mathbf{A} \mathbf{P}^{-1} \mathbf{x}, \mathbf{y})_{\mathbf{P}^{-1}} = \mathbf{y}^T \mathbf{P}^{-1} \mathbf{A}^T \mathbf{T} \mathbf{A} \mathbf{P}^{-1} \mathbf{x} = (\mathbf{x}, \mathbf{A}^T \mathbf{T} \mathbf{A} \mathbf{P}^{-1} \mathbf{y})_{\mathbf{P}^{-1}}.$$

□

Since $\hat{\mathbf{L}}$ is symmetric with respect to $(\cdot, \cdot)_{\mathbf{P}^{-1}}$, it is diagonalizable and its eigenvectors form an orthonormal basis with respect to $(\cdot, \cdot)_{\mathbf{P}^{-1}}$. Thus, we can write

$$\hat{\mathbf{L}} = \mathbf{U} \mathbf{R} \mathbf{U}^{-1} = \mathbf{U} \mathbf{R} \mathbf{U}^T \mathbf{P}^{-1}$$

with $\mathbf{R} = \text{diag}\{\rho_1, \rho_2, \dots, \rho_m\}$ being a diagonal matrix of eigenvalues, and $\mathbf{U}^T \mathbf{P}^{-1} \mathbf{U} = \mathbf{I}_m$. This decomposition can be computed once at the beginning of execution. Inserting this into eq. (18), we get

$$\begin{aligned} \mathbf{Q}_j \Phi_j \mathbf{Q}_j^T \mathbf{Z}_j + \mathbf{Z}_j \mathbf{U} \mathbf{R} \mathbf{U}^{-1} &= \mathbf{E}_1 \mathbf{B}_0 \\ \iff \Phi_j \mathbf{Q}_j^T \mathbf{Z}_j \mathbf{U} + \mathbf{Q}_j^T \mathbf{Z}_j \mathbf{U} \mathbf{R} &= \mathbf{Q}_j^T \mathbf{E}_1 \mathbf{B}_0 \mathbf{U} \\ (19) \quad \iff \Phi_j \hat{\mathbf{Z}}_j + \hat{\mathbf{Z}}_j \mathbf{R} &= \mathbf{Q}_j^T \mathbf{E}_1 \mathbf{B}_0 \mathbf{U}, \end{aligned}$$

where $\hat{\mathbf{Z}}_j = \mathbf{Q}_j^T \mathbf{Z}_j \mathbf{U} \iff \mathbf{Z}_j = \mathbf{Q}_j \hat{\mathbf{Z}}_j \mathbf{U}^{-1} = \mathbf{Q}_j \hat{\mathbf{Z}}_j \mathbf{U}^T \mathbf{P}^{-1}$. Vectorizing eq. (19), we get

$$(\mathbf{R} \otimes \mathbf{I} + \mathbf{I} \otimes \Phi_j) \text{vec}(\hat{\mathbf{Z}}_j) = \text{vec}(\mathbf{Q}_j^T \mathbf{E}_1 \mathbf{B}_0 \mathbf{U}).$$

Observe that $(\mathbf{R} \otimes \mathbf{I} + \mathbf{I} \otimes \Phi_j)$ is a diagonal matrix with diagonal entries of the form $\phi_i + \rho_k$. It follows that just as in [16, Section 5.2], one can directly compute the solution

$$(20) \quad \mathbf{Z}_j = \mathbf{Q}_j \mathbf{F}_j \mathbf{U}^T \mathbf{P}^{-1} \quad \text{where} \quad \mathbf{F}_j := (\mathbf{F}_{ik}) = \frac{\mathbf{e}_i^T \mathbf{Q}_k^T \mathbf{E}_1 \mathbf{B}_0 \mathbf{U} \mathbf{e}_k}{\phi_i + \rho_k} \in \mathbb{R}^{j \times m}.$$

REMARK 3.3. Although \mathbf{T}_j contains \mathbf{T}_{j-1} as its upper-left $(j-1)m \times (j-1)m$ submatrix, the eigendecomposition changes completely and must be recomputed at every iteration.

To make this approach computationally efficient, we must forego computing the solution approximations during the iteration. Rather, we run this iteration and use a cheap residual norm approximation to monitor convergence. In [16, Section 5.2], it is shown how to calculate an expression for the residual norm without forming the solution explicitly. This done via accumulation, and in [16, Algorithm 5], we see that, in principle, one needs to calculate the eigendecomposition of \mathbf{T}_i at each iteration i . However, the authors discuss in [16, Section 3.2] how one can calculate only the needed entries of the eigenvectors to calculate the residual norm. We note that, in our code, we do not take advantage of the trick and simply compute the full eigendecomposition. This is what we show in our description of the procedure, Algorithm 5.

Once the residual norm estimate reaches tolerance, the iteration can be stopped, and we construct the approximate solution. We construct \mathbf{Z}_j and rerun the Lanczos process to get the vectors again for constructing the solution, one block Lanczos vector at a time. This is because, from eq. (16), we can construct the approximation \mathbf{M}_j block-for-block meaning when we rerun the Lanczos iteration, we can use the blocks as they are constructed and then discard them, retaining the memory efficiency of Algorithm 5.

REMARK 3.4. In Algorithm 5 we do not perform any low-rank compression of the block Lanczos vectors. In our experiments, we determined that the block Lanczos vectors and the residuals generated when running Algorithm 5 remained numerically

ALGORITHM 5: Symmetric Sparse Sylvester Solver

```

1 Given: starting block of vectors  $\hat{\mathbf{Y}} \in \mathbb{R}^{N \times m}$ ; coefficient matrix  $\mathbf{N}^{-1}\mathbf{D}^2 \in \mathbb{R}^{N \times N}$ ; a small coefficient matrix  $\hat{\mathbf{L}} \in \mathbb{R}^{m \times m}$ ;  $\varepsilon > 0$  a convergence tolerance
2 Out: An approximation  $\mathbf{M} \in \mathbb{R}^{N \times m}$  to the solution of the Sylvester equations eq. (11)
3 Compute eigendecomposition  $\hat{\mathbf{L}} = \mathbf{U}\mathbf{R}\mathbf{U}^T$ 
4 Orthogonalize starting block in  $(\cdot, \cdot)_{\mathbf{N}}$  producing QR-factorization:  $\hat{\mathbf{Y}} = \mathbf{V}\mathbf{B}_0$ 
5  $\mathbf{V}_{old} = \mathbf{0}$ ;  $i = 0$ 
6 WHILE  $\sqrt{\gamma} > \varepsilon \|\mathbf{B}_0\|_F$  DO
7    $i \leftarrow i + 1$ 
8   /* Lanczos step ***** */
9    $\mathbf{W} \leftarrow \mathbf{N}^{-1}\mathbf{D}^2\mathbf{V}$ 
10  IF  $i > 1$  THEN
11     $\mathbf{W} \leftarrow \mathbf{W} - \mathbf{V}_{old}\mathbf{B}_i$ 
12  END
13   $\mathbf{H}_i = \mathbf{V}^T\mathbf{N}\mathbf{W}$ 
14   $\mathbf{W} \leftarrow \mathbf{W} - \mathbf{V}\mathbf{H}_i$ 
15   $\mathbf{V}_{old} \leftarrow \mathbf{V}$ 
16  Orthogonalize  $\mathbf{W}$  in  $(\cdot, \cdot)_{\mathbf{N}}$  producing QR-factorization:  $\mathbf{W} = \mathbf{V}\mathbf{B}_{i+1}$ 
17  /* computing residual norm according to [16, Section 5.2]
18  ***** */
19   $\gamma \leftarrow 0$ 
20  Compute eigendecomposition  $\mathbf{T}_i = \mathbf{Q}_i\Phi_i\mathbf{Q}_i^T$ 
21   $\mathbf{S} \leftarrow (\mathbf{U}^T\mathbf{B}_0^T)(\mathbf{E}_1^T\mathbf{Q}_i)$ 
22   $\mathbf{J} \leftarrow (\mathbf{Q}_i\mathbf{E}_m)\mathbf{B}_{i+1}^T$ 
23  FOR  $j = 1, 2, \dots, m$  DO
24     $\mathbf{K} \leftarrow \rho_j\mathbf{I} + \Phi_i$ 
25     $\gamma \leftarrow \gamma + \|(\mathbf{e}_j^T\mathbf{S})\mathbf{K}^{-1}\mathbf{J}\|_2^2$ 
26  END
27 END
28 /* constructing approximation coefficients entry-wise ***** */
29  $\mathbf{F} = \mathbf{0} \in \mathbb{R}^{i \times m}$ 
30 FOR  $k = 1, 2, \dots, i$  DO
31   FOR  $\ell = 1, 2, \dots, m$  DO
32      $\mathbf{F}_{k\ell} = \frac{\mathbf{e}_k^T\mathbf{Q}_\ell^T\mathbf{E}_1\mathbf{B}_0\mathbf{U}\mathbf{e}_\ell}{\phi_k + \rho_\ell}$ ; see (20)
33   END
34 END
35  $\mathbf{Z} = \mathbf{Q}_i\mathbf{F}\mathbf{U}^T$ 
36 /* rerun Lanczos to assemble solution ***** */
37  $\mathbf{M} = \mathbf{0}$ 
38  $\mathbf{V} \leftarrow \hat{\mathbf{Y}}\mathbf{B}_0^{-1}$ 
39  $\mathbf{V}_{old} = \mathbf{0}$ 
40 FOR  $j = 1, 2, \dots, i$  DO
41    $\mathbf{M} \leftarrow \mathbf{M} + \mathbf{V}\mathbf{G}_j$ , according to (16)
42   /* Lanczos step using already-computed coefficients ***** */
43    $\mathbf{W} \leftarrow \mathbf{N}^{-1}\mathbf{D}^2\mathbf{V}$ 
44   IF  $j > 1$  THEN
45      $\mathbf{W} \leftarrow \mathbf{W} - \mathbf{V}_{old}\mathbf{B}_j$ 
46   END
47    $\mathbf{W} \leftarrow \mathbf{W} - \mathbf{V}\mathbf{H}_j$ 
48    $\mathbf{V}_{old} \leftarrow \mathbf{V}$ 
49    $\mathbf{V} \leftarrow \mathbf{W}\mathbf{B}_{j+1}^{-1}$ 
50 END
51 Output  $\mathbf{M}$ 

```

full rank (i.e., rank 4). Thus, we do not pursue a strategy of compression in our Sylvester solver.

4. EVALUATION AND APPLICATION

We have proposed using two approaches described in the literature for solving this source separation problem by exploiting the Kronecker structure of the linear system. In the first method, we employ conjugate gradients applied directly to the Kronecker form of the system, and the structure is exploited to obtain a matrix-free iteration. In the latter method, we similarly exploit the Sylvester formulation of the problem using a Lanczos-based iterative method, and we are again able to do this in a matrix-free way.

In this section, we demonstrate with our numerical results that both approaches are viable for the underlying application problem. In theory, though, we should expect better performance from the method based on the Sylvester formulation. This has been shown in [17]

Three implementations (two variants of the conjugate gradient approach and the Sylvester method) are applied to BOTH simulated data of different sizes (allowing for evaluation of the actual error) as well as actual Planck full sky maps. Results are compared in terms of time cost, memory usage, and accuracy. Code profiling explores how these requirements for different aspects of the algorithm change with problem size.

The experiment is designed as follows. The 3 solutions were run with simulated data having different values of N_{side} . Since the source \mathbf{S} is specified in each simulation, this allows us to compare the results of the algorithms with the true solution of the simulated problem. The problem size is specified as the HEALPix level from 1 to 10. Recalling that the solution dimension at level h is $m \times N_{side} = m \times 12 \times 4^h$, hence increasing the level by 1 increases the dimension of the solution by 4.

For the simulated and Planck data, $m = 4$ sources and $n = 9$ images were assumed, as discussed in Appendix B. Data were simulated by specifying values for the source vector \mathbf{S} (for simplicity, these are generated as independent samples from a normal distribution), and the matrix \mathbf{A} and vector \mathbf{T} were defined as in Appendix B). That allows the data vector \mathbf{Y} to be randomly generated as in Equation 1.

Code was written in Python and implemented on a cluster with specification described in Table 1.

Property	Value
Architecture	64
Number of Nodes	100
Ram per node	24GB
RAM	2.4TB
Clock Speed	2.66GHz
Total number of cores	1200
Theoretical Peak Performance	12.76TF
Operating System	Scientific Linux 6.x
Allocated Memory	50GB
Allocated Nodes	2
Allocated Cores per Node	12

TABLE 1. Specification of the machine used in the experiments.

4.1. ACCURACY. Figure 1 shows the relationship between the source vector of the random-generated data and the solution produced by the Conjugate Gradient method on our linear system for simulated data with $h = 6$ or $N_{side} = 49,152$. They almost matched with an error margin (defined to be largest absolute error across all components of the source vector divided by the average value of the source vector) of 0.4%. Similar results are seen for data of other sizes.

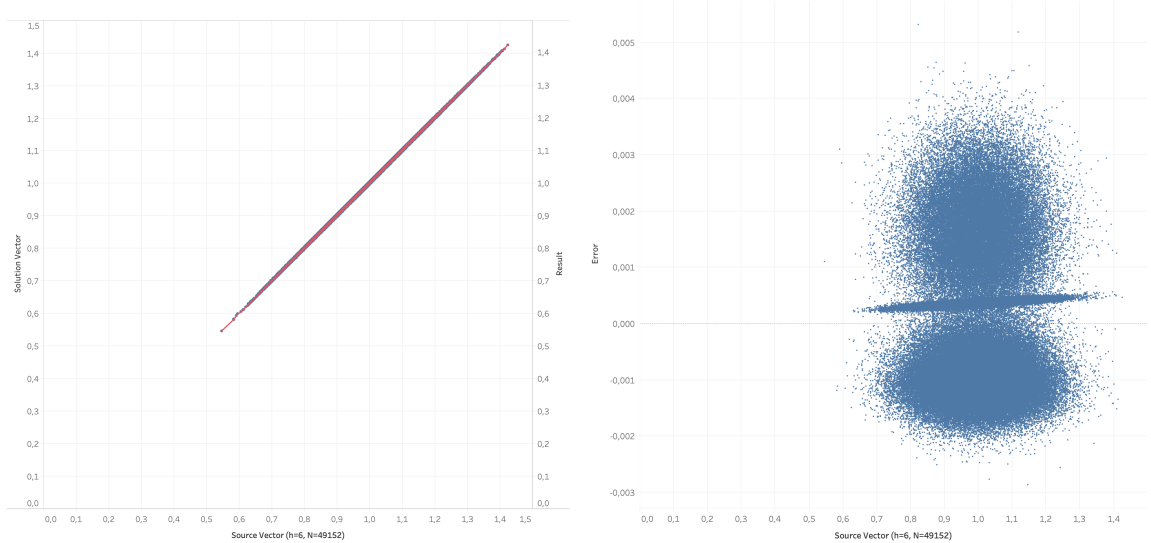


FIGURE 1. Solution accuracy. Scatter plot of components of the true source vector \mathcal{S} versus the solution vector (left) and source vector versus the error (right).

4.2. TIME AND MEMORY USAGE. Figure 2 shows the time cost (in seconds) while running the Conjugate Gradient and Sylvester methods on simulated and Planck data, as a function of HEALPix level and the data size; Appendix A explains that HEALPix level h means a data size of 4^h , hence signifies log data size. The difference between Planck and simulated data is due to the longer time that it took to load in the Planck data from a file than it took to simulate data of the same size. However, the main difference is that the Sylvester method is consistently faster, taking only about 15% of the time of the Conjugate Gradient approach for the larger data sizes. In both cases, the algorithm demonstrates a close to linear complexity with the data size N , a substantial improvement over exact solution methods that are at least quadratic with N . We hypothesize that the superior performance of the Sylvester block Krylov method over the CG method applied directly to the Kronecker-structured problem is due both to conditioning issues reported in [17] as well as the superior data movement characteristics (higher computational intensity) often exhibited by block-Krylov-subspace-based methods; see, e.g., [2].

Figure 3 show the total memory usage (in MB) while running the Conjugate Gradient and Sylvester methods on simulated and Planck data. We see that the Sylvester method’s memory requirements are about half of that of the Conjugate Gradient, the former needing about 47GB for HEALPix level 10, which is the size of the Planck satellite data.

4.3. CODE PROFILING. Figure 4 is a break down of the computation time and memory use, as a function of problem size, by the functions in the code that used the most of these resources. A description of these functions is given in Table 2. For time, the top 4 functions at HEALPix level 10 are plotted, while for memory there were only 3 functions that accounted for almost all of the memory use. For memory, unsurprisingly it is the functions that load or make use of all of the data that dominate resources. For time, we see that mapping and computation around the **D** matrix dominate the computation time. This suggests that efforts to further speed up the algorithm should focus on this task. Encouragingly, operations around the **D** matrix are well suited to parallelisation [23, 7].

4.4. COMPARISON WITH APPROACH FROM [4]. We construct the sparse-dense form of the Sylvester equation and apply Algorithm 3 to the Planck dataset. For this dataset, $m = 4$ and $N = 12 \times 4^h, h = 1, 2, \dots, 10$. For the largest size of the problem, $\mathbf{H} \in \mathbb{R}^{12,582,912 \times 12,582,912}$, wherein we remind the reader that this matrix is the large, sparse matrix appearing in (12).

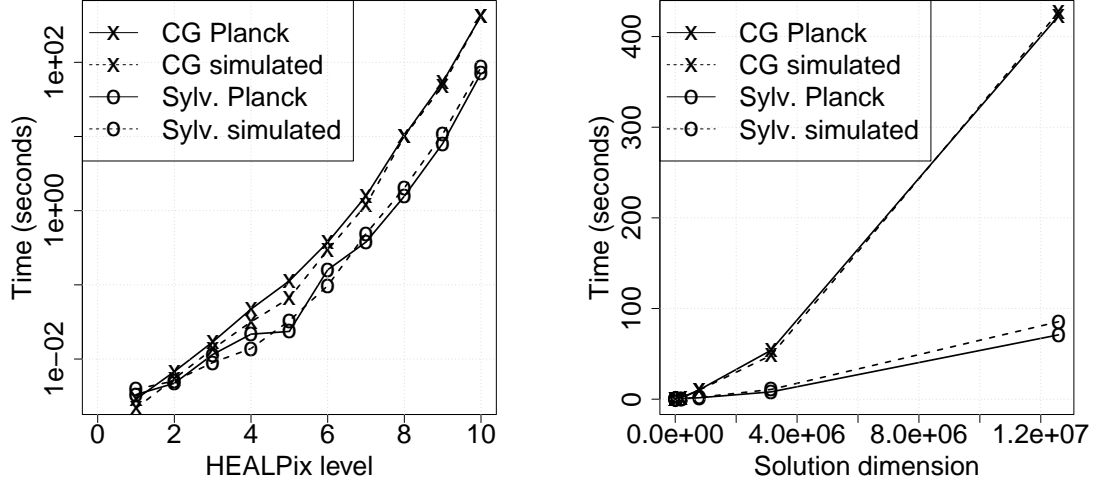


FIGURE 2. Running time (in seconds) by HEALPix level (left) and data size (right).

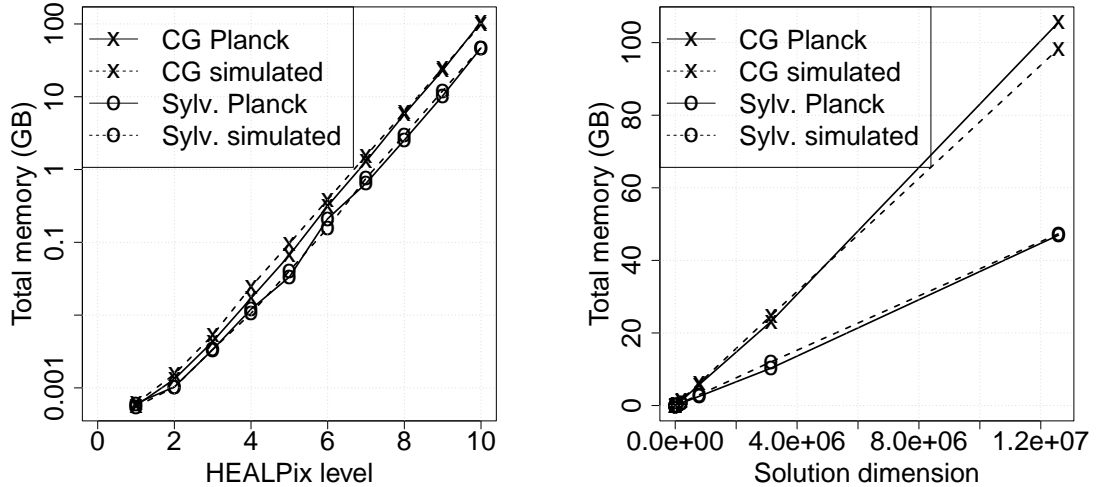


FIGURE 3. A comparison of total memory usage by HEALPix level (left) and data size (right) for Algorithm 2 (CG) versus Algorithm 5 (Lanczos-Sylvester - i.e., Sylv.) for both synthetic data and actual Planck satellite data.

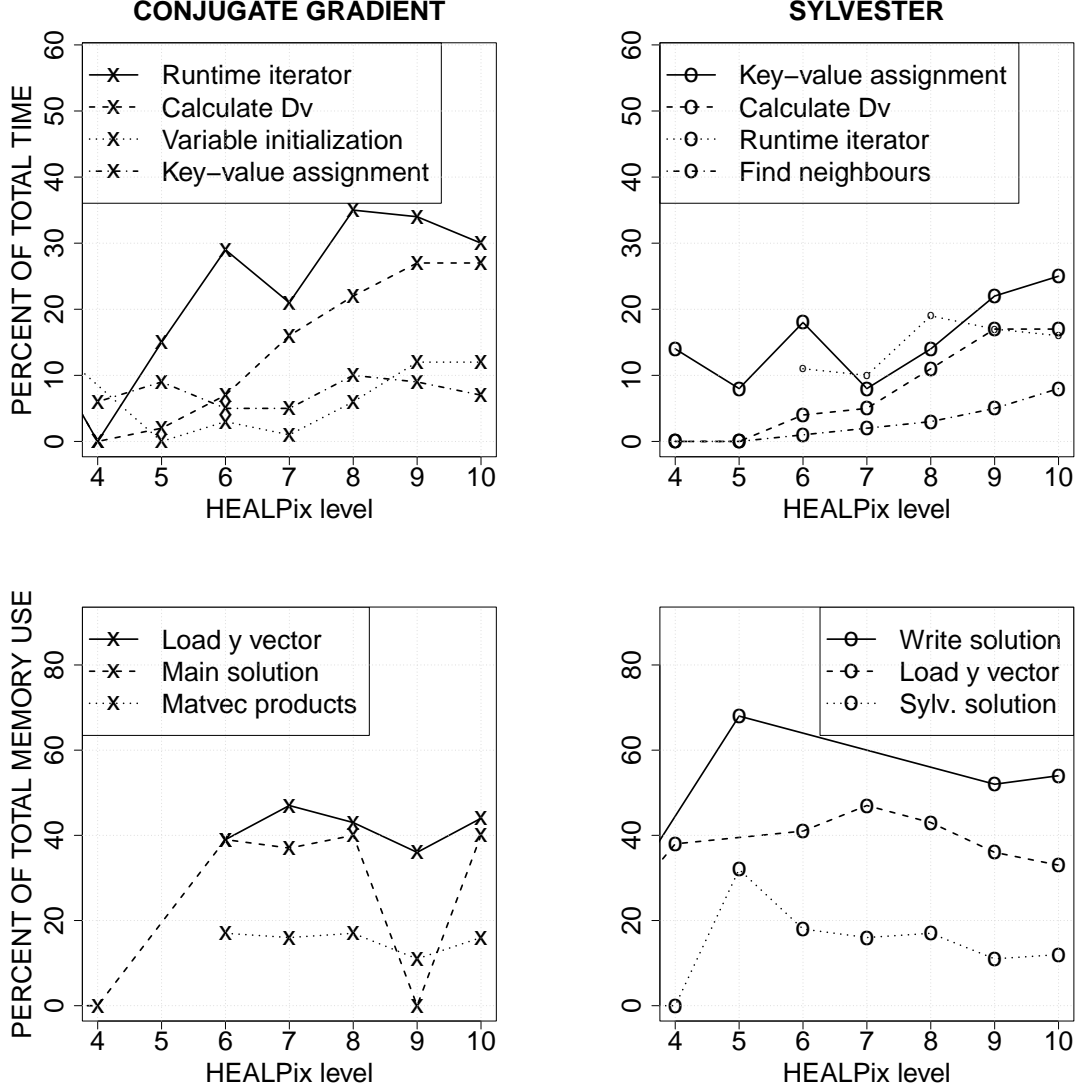


FIGURE 4. Code profiling. The functions that consume the most resources as a function of problem size. The top row is percentage of total computation time and the bottom row is percentage of maximum memory use. Table 2 provides more information on the functions. Sylv. refers to Algorithm 5.

The results in terms of accuracy and running time of our Sylvester approach Algorithm 5 and the approach from [4], (i.e., Algorithm 3) are shown in Table 3 a and b, respectively. The Sparse-Dense method shows significant advantages in accuracy with a comparable running time. However, we observed that for larger Planck data sizes, the solve time for Algorithm 3 grew quadratically. Further investigation revealed that unlike for the problems discussed in [4], the SuperLU inner linear

Function	Description
Calculate D_v	Implementation of Algorithm 1.
Find neighbours	Identify neighbouring pixel indices in the HEALPix partition.
Runtime iterator	A system function to determine the next item to process, used to p
Key-value assignment	A system function to assign a value to a key (string) in the code.
Variable initialization	Define all variables for the problem and allocate memory.
Load y vector	Self explanatory.
Main solution	Managing the main loop of code.
Matvec products	Implementation of the calculations described in Section 3.1.
Sylvester solution	Main while loop of Algorithm 5.
Write solution	Self explanatory.

TABLE 2. Definition of functions listed in Figure 4.

solver was not effective at reducing solve time growth rate. We note that we did try different sparse direct solvers (UMFPACK, SuperLU) and an iterative method (Conjugate Gradient), all within the scipy Python library. The SuperLU solver proved to be the most efficient and accurate one for our specific data. We tried multiple approaches with this code to reduce the growth in run-time, but the growth in runtime remained quadratic. Further investigation of this issue is out of the scope of our paper. In comparison, our method is demonstrated to be efficient, even for the full size of the Planck dataset.

5. CONCLUSION

In this paper we have described a particular statistical model and a Bayesian learning algorithm to fit it to data of high dimension, motivated by the source separation problem for Cosmic Microwave Background. The computational bottleneck of the implementation of this algorithm is to solve a linear system and we have shown 2 approximate solvers applied to this learning algorithm that make use of a Krylov subspace. We have shown that both approaches produce solutions at the size of Planck data (currently the most detailed all-sky data that we have) in a reasonable computation time with reasonable memory requirements. We show that the solution of this problem admits a representation as the solution of sparse-dense Sylvester equations. For problems of the size generated by the real scientific problem from Planck satellite data, our experiments indicate that standard approaches for sparse-dense problems become too costly to apply. By instead using a modified version of the approach suggested in [16, Section 5.2], our approach to solving

Level (h)	N	Lanczos-Sylvester	Sparse-Dense Method
1	48	1.72e-06	2.23e-10
2	192	4.21e-06	3.28e-10
3	768	7.02e-06	4.73e-10
4	3072	4.86e-06	6.19e-10
5	12288	8.62e-06	5.85e-09
6	49152	1.08e-06	2.19e-10
7	196608	1.35e-06	2.6e-09
8	786432	1.58e-06	1.93e-09
9	3145728	1.74e-06	1.21e-09
10	12582912	4.23e-06	—

(A) Residual Comparison

Level (h)	N	Lanczos-Sylvester	Sparse-Dense Method
1	48	0.003	0.001
2	192	0.004	0.006
3	768	0.012	0.035
4	3072	0.021	0.3
5	12288	0.023	0.755
6	49152	0.159	4.35
7	196608	0.377	37.312
8	786432	1.566	301.698
9	3145728	8.042	6948.4228
10	12582912	70.930	—

(B) Running Time Comparison

TABLE 3. Comparison using Planck Data (with $m = 4$ sources), between the sparse-dense method proposed in [4] and the Lanczos-Sylvester method adapted from [16, Section 5.2]. The Sparse-Dense method shows significant advantages in accuracy with a comparable running time for smaller problems. However, for larger problems, the solve-time required by the sparse-dense method, even when implemented using Super-LU as the inner solver grows like $\mathcal{O}(N^2)$ rather than $\mathcal{O}(N)$ for these problems. This causes the sparse-dense solver to run so long that we aborted the $h = 10$ experiment.

the Sylvester equations has a significant advantage in computation time, taking only about one-sixth of the time of the conjugate gradient approach for larger data sizes. This highlights the advantage of exploiting the Sylvester structure over treating the Kronecker-structured problem directly. The almost-linear complexity of the algorithm implies that it will also be practical to use these approaches on any future data that is of larger size.

We note that a full implementation of the statistical solution also learns about the model parameters, such as those that define the \mathbf{A} and \mathbf{Q} matrices. In this

paper those have been assumed fixed, in order to focus on the issue of the linear system. Since there are a small number of these parameters, the usual solution involves repeatedly solving the linear system for different combinations of values of these parameters and building up a picture of which fit the data best. In Bayesian learning this can be done through the integrated nested Laplace approximation [22]. Having to solve the linear system multiple times makes the need for an efficient solver even more important. Thus, further improvements to accelerate the solution should be explored. For example, subspace augmentation and recycling techniques (see, e.g., [28] and references therein) would have the potential to accelerate the solution of multiple systems needed to learn the model parameters.

ACKNOWLEDGEMENTS

The authors would like to thank the anonymous referees for their constructive critiques and suggestions, which greatly improved this manuscript. The authors affirm they have no conflicts of interest.

APPENDIX A. HEALPIX

HEALPix (Hierarchical Equal Area isoLatitude Pixelation) is a multi-resolution partition of the sphere into elements or pixels of equal area, although not the same shape. It was originally used to provide a discretization of all-sky observations done in connection with CMB but it is now used in many other fields. As of writing, an active website of resources is available at <https://healpix.sourceforge.io/>.

The base partition is into 12 elements. Successively more refined levels of the partition are made by dividing an element into 4 new elements (see Figure 5). Taking the base partition to be level 0, the HEALPix partition at level h therefore has 12×4^h elements. For WMAP data, level 9 was used while for Planck a higher resolution of level 10 was possible, hence there are $12 \times 4^{10} = 12,582,912$ pixels in each image. HEALPix software supports data input and output, visualization and features like identifying neighbouring pixel indices and the indices of pixels in discs, triangles, polygons and strips.

Most analyses with data indexed using HEALPix will do separate analyses on each of the 12 base partition elements because functions such as identifying neighbouring

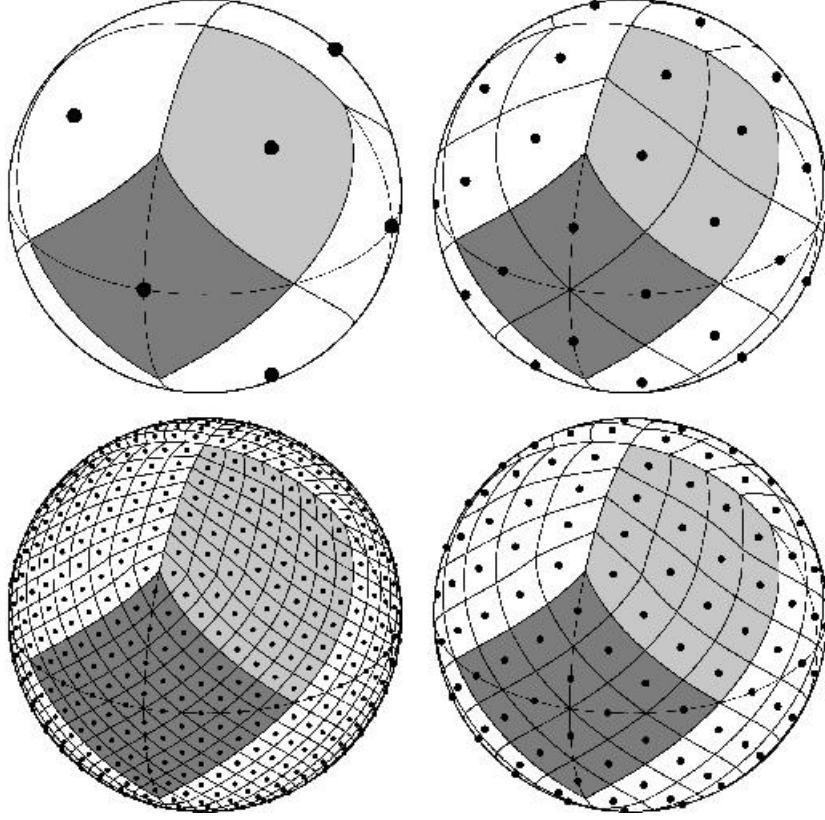


FIGURE 5. HEALPix partitions. Clockwise from top left: the base partition into 12 pixels, then level 1, 2 and 3 (48, 192 and 768 pixels). Taken from <https://healpix.sourceforge.io/>.

pixels are only available within them. That is what is done here. So our source separation on data at HEALPix level h will consist of 12 independent analyses with $N = 4^h$.

APPENDIX B. THE MATRIX \mathbf{A} IN THE CMB SOURCE SEPARATION PROBLEM

The matrix \mathbf{A} gives the coefficients of the assumed linear relationship between sources and observed brightnesses (Equation 1). It is an $n \times m$ matrix and so typically small e.g. $n = 9$ for Planck data and we might use $m = 4$ or 5. The element A_{kl} can be interpreted as the contribution of the l th source to the k th map. It is called the mixing matrix in the context of source separation. CMB is indexed as the first source, so the first column of A gives the contributions of CMB. In this work, 3 other sources are assumed, in order: synchrotron radiation, galactic dust and free-free emission.

The first thing to note is the well-known property of source separation solutions (and more generally factor analysis) that \mathbf{A} and \mathbf{s} are unique only up to an orthogonal transformation. In the CMB application, uniqueness is gained by considering the separation in units of the CMB intensity, so that the first column of \mathbf{A} is a vector of 1's.

For the other columns of \mathbf{A} , the physics of the sources are used to give expressions for the A_{kl} . For synchrotron emission, a straight power law can be used:

$$A_{k2} = c(\nu_k) \left(\frac{\nu_k}{\nu_0} \right)^{\kappa_s},$$

for a reference frequency ν_0 at which the source maps will be expressed (for Planck data this is usually the 4th frequency at 100 GHz) and $c(\nu) = (e^\psi - 1)^2 / \psi^2 e^\psi$, where $\psi = h\nu/k_B T_1$ with h and k_B are the Planck and Boltzmann constants and $T_1 = 18.1\text{K}$. The parameter κ_s is known as the spectral index and is typically somewhere in the range $(-2.3, -3.0)$. Here we assume $\kappa_s = -2.65$.

For galactic dust, a modified black body spectrum is used, multiplied by a power law,

$$A_{k3} = c(\nu_k) \frac{B(\nu_k)}{B(\nu_0)} \left(\frac{\nu_k}{\nu_0} \right)^{\kappa_d},$$

where $B(\nu_k) = \nu_k / [\exp(h\nu_k/k_B T_1) - 1]$. The spectral index for dust κ_d is typically in the range $(1, 2)$. Here we assume $\kappa_d = 1.5$.

For free-free emission, a straight power law with known spectral parameter of -2.14 is used:

$$A_{k4} = c(\nu_k) \left(\frac{\nu_k}{\nu_0} \right)^{-2.14}.$$

For Planck data, where the 9 maps are for microwave frequencies at 30, 44, 70, 100, 143, 217, 353, 545 and 857 GHz, this yields

$$\mathbf{A} = \begin{pmatrix} 1.000 & 24.314 & 0.181 & 13.158 \\ 1.000 & 8.817 & 0.315 & 5.801 \\ 1.000 & 2.581 & 0.612 & 2.151 \\ 1.000 & 1.006 & 1.006 & 1.006 \\ 1.000 & 0.392 & 1.630 & 0.471 \\ 1.000 & 0.132 & 2.783 & 0.196 \\ 1.000 & 0.038 & 4.931 & 0.072 \\ 1.000 & 0.013 & 7.704 & 0.032 \\ 1.000 & 0.005 & 11.337 & 0.015 \end{pmatrix}.$$

We also need the vector \mathbf{T} in the definition of \mathbf{C} . For this application, the values are:

$$\mathbf{T} = \text{diag}\{629881.6, 694444.4, 783146.7, 12755102.0, 30864197.5, 30864197.5, 30864197.5, 30864197.5, 30864197.5\}.$$

APPENDIX C. THE INTRINSIC GAUSSIAN MARKOV RANDOM FIELD

A full derivation of the intrinsic Gaussian Markov random field (IGMRF) and its properties can be found in [21, Chapter 3], of which below is a brief summary.

A set of random variables $X = (X_1, \dots, X_N)$ is a *Markov random field* if

- Each variable X_i has a neighbourhood set $\eta_i \subset \{1, \dots, N\}$ that satisfies the properties: $i \notin \eta_i$ and $j \in \eta_i$ iff $i \in \eta_j$. Intuitively, when the X_i are values of pixels in a 2-dimensional image, η_i is the indices of the neighbour pixels of pixel i . In this application using the HEALPix tesslation, the neighbours are the 4 pixels that share a common edge (as can be seen in Figure 5).
- Each X_i is independent of the other variables in the set given its neighbours. In other words $p(x_i | \{x_j | j \neq i\}) = p(x_i | \{x_j | j \in \eta_i\})$.

Under quite general conditions, the joint probability distribution $p(x_1, \dots, x_n)$ is uniquely defined by the set of conditional distributions $p(x_i | \{x_j | j \in \eta_i\})$, $i = 1, \dots, N$, of each random variable given its neighbours. For the case of a 2-dimensional grid, the effect of these assumptions is that the values of nearby random variables on the grid are more correlated than those that are far away, and so realizations of the set

of random variables are more spatially smooth than the case where each variable is independent.

When these conditional distributions are Gaussian, the joint distribution is a multivariate Gaussian with some mean vector $\boldsymbol{\mu}$ and covariance matrix $\boldsymbol{\Sigma}$, and it is known as a *Gaussian Markov random field* (GMRF). The inverse of the covariance matrix, $\mathbf{Q} = \boldsymbol{\Sigma}^{-1}$, known as the precision matrix, has a nice structure since an off-diagonal element is zero if and only if the corresponding random variables are not neighbours:

$$j \notin \{i\} \cup \eta_i \iff Q_{ij} = 0.$$

In most cases, including ours, since the number of neighbours is small relative to N , \mathbf{Q} will be sparse.

Finally, we get to the intrinsic GMRF. The key property of these models is that they are improper – they look like GMRFs but their joint probability distribution takes the form of a multivariate Gaussian but with a precision matrix that is not of full rank. Hence their joint distribution is not a properly defined probability density function. This may seem to be a disqualifying property for a probability model but in fact (a) they model properties of the random variables that can be useful and (b) when used as a prior distribution, as in this application, the resulting posterior distribution is very often a properly defined probability distribution.

The vector of random variables $X = (X_1, \dots, X_N)$ is an *improper GMRF* of rank $N - k$ with parameters $(\boldsymbol{\mu}, \mathbf{Q})$ if its density is of the form:

$$p(x) = (2\pi)^{-0.5(N-k)} (|\hat{\mathbf{Q}}|)^{0.5} \exp(-0.5(\mathbf{x} - \boldsymbol{\mu})^T \mathbf{Q}(\mathbf{x} - \boldsymbol{\mu})), \quad x \in \mathbb{R}^N,$$

where \mathbf{Q} is an $N \times N$ semi-positive definite matrix of rank $N - k > 0$ and $|\hat{\mathbf{Q}}|$ is a generalised determinant, being the product of the $N - k$ non-zero eigenvalues of \mathbf{Q} .

The properties of such a construction are discussed in great detail in [21]. A specific example of an IGMRF, that we use in this work, is where $\boldsymbol{\mu} = \mathbf{0}$ and $\mathbf{Q} = \varphi \mathbf{D}^T \mathbf{D}$, for $\varphi > 0$ and \mathbf{D} an $N \times N$ matrix that encodes the neighbourhood structure,

$$(21) \quad D_{ij} = \begin{cases} 1, & \text{if } i \in \eta_j, \\ 0, & \text{otherwise,} \end{cases}$$

giving \mathbf{Q} a rank of $N - 1$. One can show that under this definition of \mathbf{Q} , the distribution of X_i given its neighbours $\{X_j | j \in \eta_i\}$ is Gaussian with mean equal to the average of its neighbours. This makes a realisation of X somewhat smooth, in that neighbouring values in the HEALPix lattice are more likely to take similar values than those that are further apart. Another property of this construction is that there is no mean level specified -- although $\boldsymbol{\mu} = \mathbf{0}$ this is not the 'mean' of X as it is not a properly defined probability distribution. The construct only gives properties of the relationship between neighbouring values in the lattice, not about their overall level. This is useful if all that one wants to model for X is this smooth spatial property, and not commit to a particular mean level a priori.

That is the approach that we have taken in modelling the sources in our separation problem. Each source is modelled as an independent IGMRF, with the l th source having parameters $\mu_l = 0$ and $\mathbf{Q}_l = \varphi_l \mathbf{D}^T \mathbf{D}$, with \mathbf{D} defined as in Equation 21. In this paper we have fixed $\varphi_l = 1$ for each source. Stacking these independent sources into the vector \mathbf{S} yields a Gaussian form with mean 0 and a block-diagonal precision matrix $\mathbf{Q} = \text{diag}(\mathbf{Q}_1, \dots, \mathbf{Q}_m)$.

REFERENCES

- [1] E. Aune, D. P. Simpson, and J. Eidsvik. "Parameter estimation in high dimensional Gaussian distributions". In: . 24 (2014), pp. 247–263.
- [2] Allison H. Baker, John M. Dennis, and Elisabeth R. Jessup. "On improving linear solver performance: a block variant of GMRES". In: . 27.5 (2006), pp. 1608–1626. issn: 1064–8275. doi: 10.1137/040608088.
- [3] D. Bartholomew, M. Knott, and I. Moutaki. . Third. Chichester: John Wiley & Sons, Ltd., 2011.
- [4] Peter Benner, Martin Köhler, and Jens Saak. "Sparse-Dense Sylvester Equations in H_2 -Model Order Reduction". In: MPIMD/11–11 (Jan. 2011). Last accessed at <https://csc.mpi-magdeburg.mpg.de/preprints/2011/MPIMD11-11.pdf> on 17 October 2023.
- [5] C. M. Bishop. . Second. Springer, 2007.

- [6] Erik G Boman, Andrew J Higgins, and Daniel B Szyld. "Optimal size of the block in block GMRES on GPUs: computational model and experiments". In: . 92.1 (2023), pp. 119–147. doi: 10.1007/s11075-022-01439-z.
- [7] G. W. Burr et al. "Neuromorphic computing using non-volatile memory". In: . 2.1 (2017), pp. 89–124.
- [8] J. Delabrouille et al. "Exploring cosmic origins with CORE: survey requirements and mission design". In: . 2018.04 (2018), pp. 014–014.
- [9] Roland W. Freund. "Solution of shifted linear systems by quasi-minimal residual iterations". In: . de Gruyter, Berlin, 1993, pp. 101–121. isbn: 3-11-013784-4.
- [10] John R. Gilbert and Robert Schreiber. "Highly Parallel Sparse Cholesky Factorization". In: . 13.5 (Sept. 1992), pp. 1151–1172. doi: 10.1137/0913067. url: <https://doi.org/10.1137%2F0913067>.
- [11] K. M. Górski et al. "HEALPIX – a framework for high resolution discretization, and fast analysis of data distributed on the sphere". In: . 622 (2005), p. 759.
- [12] X.S. Li et al. . Tech. rep. LBNL-44289. <https://portal.nersc.gov/project/sparse/superlu/ug.pdf> Last update: June 2018. Lawrence Berkeley National Laboratory, Sept. 1999.
- [13] Xiaoye S. Li. "An Overview of SuperLU: Algorithms, Implementation, and User Interface". In: . 31.3 (Sept. 2005), pp. 302–325.
- [14] Xiaoye S. Li and James W. Demmel. "SuperLU_DIST: A Scalable Distributed-Memory Sparse Direct Solver for Unsymmetric Linear Systems". In: . 29.2 (June 2003), pp. 110–140.
- [15] Dianne P. O’Leary. "The block conjugate gradient algorithm and related methods". In: . 29 (1980), pp. 293–322.
- [16] Davide Palitta and Valeria Simoncini. "Computationally enhanced projection methods for symmetric Sylvester and Lyapunov matrix equations". In: . 330 (2018), pp. 648–659. issn: 0377-0427. doi: 10.1016/j.cam.2017.08.011.
- [17] Davide Palitta and Valeria Simoncini. "Optimality properties of Galerkin and Petrov-Galerkin methods for linear matrix equations". In: . 48.4 (2020), pp. 791–807. issn: 2305-221X.

- [18] J. Papež, L. Grigori, and R. Stompor. "Accelerating linear system solvers for time-domain component separation of cosmic microwave background data". In: . 638 (June 2020), A73. issn: 1432-0746. doi: 10.1051/0004-6361/202037687. URL: <http://dx.doi.org/10.1051/0004-6361/202037687>.
- [19] Michael L. Parks, Kirk Soodhalter, and Daniel B. Szyld. . Tech. rep. 16-04-04. Department of Mathematics, Temple University, Apr. 2016.
- [20] A. Penzias and R. W. Wilson. "A Measurement of the flux density of CAS A at 4080 Mc/s". In: . (1965), pp. 1149-1154.
- [21] H. Rue and L. Held. . Boca Raton, Fl.: Chapman and Hall/CRC, 2005.
- [22] H. Rue, S. Martino, and N. Chopin. "Approximate Bayesian inference for latent Gaussian models using integrated nested Laplace approximations". In: . 71.2 (2009), pp. 319-392.
- [23] Y. Saad. "Krylov subspace methods on supercomputers". In: . 10 (1989), pp. 1200-1232.
- [24] Yousef Saad. . Second. Philadelphia: SIAM, 2003.
- [25] V. Simoncini. "Computational methods for linear matrix equations". In: . 58.3 (2016), pp. 377-441. issn: 0036-1445.
- [26] Valeria Simoncini and Daniel B. Szyld. "Recent computational developments in Krylov subspace methods for linear systems". In: . 14.1 (2007), pp. 1-59. issn: 1070-5325. doi: 10.1002/nla.499.
- [27] D. P. Simpson. "Krylov subspace methods for approximating functions of symmetric positive definite matrices with applications to applied statistics and anomalous diffusion". PhD thesis. Queensland University of Technology, 2008.
- [28] Kirk M. Soodhalter, Eric de Sturler, and Misha E. Kilmer. "A survey of subspace recycling iterative methods". In: . 43.4 (Sept. 2020). issn: 1522-2608. doi: 10.1002/gamm.202000016. URL: <http://dx.doi.org/10.1002/gamm.202000016>.
- [29] Henk A. van der Vorst. . Vol. 13. Cambridge Monographs on Applied and Computational Mathematics. Reprint of the 2003 original. Cambridge University Press, Cambridge, 2009, pp. xiv+221. isbn: 978-0-521-18370-3.

(D. Pham) SCHOOL OF COMPUTER SCIENCE AND STATISTICS TRINITY COLLEGE DUBLIN
COLLEGE GREEN, DUBLIN 2 IRELAND

Email address: phamd@tcd.ie

(K. M. Soodhalter) SCHOOL OF MATHEMATICS TRINITY COLLEGE DUBLIN COLLEGE GREEN,
DUBLIN 2 IRELAND

Email address: ksoodha@maths.tcd.ie

URL: <https://math.soodhalter.com>

(S. Wilson) SCHOOL OF COMPUTER SCIENCE AND STATISTICS TRINITY COLLEGE DUBLIN
COLLEGE GREEN, DUBLIN 2 IRELAND

Email address: SWILSON@tcd.ie